Tailoring THz antiferromagnetic resonance of NiO by cation substitution

Takahiro Moriyama,[1,*] Kensuke Hayashi,[2] Keisuke Yamada,[2] Mutsuhiro Shima,[2] Yutaka Ohya,[2] and Teruo Ono[1,3]

[1]*Institute for Chemical Research, Kyoto University, Gokasho, Uji, Kyoto, 611–0011, Japan*

[2]*Department of Materials Science and Processing, Graduate School of Natural Science and Technology, Gifu University, Yanagido, Gifu City, Gifu 501–1193, Japan*

[3]*Center for Spintronics Research Network, Graduate School of Engineering Science, Osaka University, Toyonaka, Osaka 560-8531, Japan*

(Received 9 March 2020; revised 21 May 2020; accepted 16 June 2020; published 7 July 2020)

Antiferromagnets generally have a quite high magnetic resonance, as known as the antiferromagnetic resonance, whose frequency goes up to the THz range. They are one of the few materials that can magnetically couple to THz electromagnetic waves and are therefore important materials for THz technologies. In this work, we demonstrate that the THz resonance properties, such as resonant frequency and the Q factor, of antiferromagnetic NiO can be controlled over a wide range by substituting the Ni^{2+} cation with various different cations. Our discussion extends to the trends of how different substitute cations Mn^{2+}, Li^{+}, and Mg^{2+} impact the resonant properties, which suggests a guideline for designing antiferromagnetic THz materials.

DOI: 10.1103/PhysRevMaterials.4.074402

Antiferromagnets are considered key THz materials owing to their magnetic resonant frequency in THz range [1,2]. While ferromagnetic materials are now widely used in passive microwave components in a GHz range, such as inductors and microwave absorbers [3], antiferromagnets can likewise find a great use in similar passive components in a THz range foreseeing the post 5G technology [4]. Moreover, recent theoretical and experimental efforts in antiferromagnetic spintronics [5,6] push forward the development of active THz devices, such as ultrafast memory devices [7] and THz spin oscillators [8,9]. NiO is one of the prototypical collinear antiferromagnets and is regarded as a charge-transfer type insulator [10,11]. It has been historically and widely investigated in both physics and application points of view [12–19]. The crystalline and magnetic structure are illustrated in Fig. 1(a). It has a rock-salt structure (point group: $m\bar{3}m$) above the Néel temperature $T_N = 523$ K and it sustains a slight rhombohedral distortion when the antiferromagnetic order emerges below T_N (point group: $\bar{3}m$). In the ground state below T_N, the Ni^{2+} spins align ferromagnetically in a {111} plane and antiferromagnetically coupled between adjacent {111} planes due to the superexchange of the Ni $3d$ orbitals through the O $2p$ orbitals [20]. This preferential orientation of spins results in a strong magnetic *easy-plane* anisotropy in a {111} plane and a weak three-fold *in-plane* anisotropy in the $\langle 11\bar{2}\rangle$ directions in the {111} plane [16].

In contrast to the magnetic structure, the electronic structure is still elusive and is a long-standing debate in theoretical condensed matter physics [10–13,17]. Nevertheless, it is empirically known to be a wide-gap p-type semiconductor (the bandgap of ∼4.0 eV [21]) with excellent chemical stability. Its electrical and chemical properties attract the interest of various applications, such as highly efficient hole transport layers for organic solar cells [22] and ultraviolet optics [23]. A wide variety of ionic elements have been doped into NiO to tailor the electric properties as well as the bandgap. For instance, it has been reported that substituting the Ni^{2+} site with a monovalent cation, such as Li^{+}, further increases the hole conductivity [24,25]. On the other hand, Mg^{2+} doping increases the bandgap associating with expansion of the lattice parameter [26,27].

Despite extensive explorations of electrical and magnetic properties in pure NiO as well as those composite systems since the early days, there has been little study particularly focusing on the effect of various dopants on the antiferromagnetic resonance properties [28,29]. Considering the strong correlation of magnetic and electric properties in this material, it is expected that doping with various ions would bring about rather drastic influences on antiferromagnetic dynamics. Is it also interesting and quite useful in the practical point of views mentioned above, if one can tailor the antiferromagnetic resonant frequency as well as the Q factor of the resonance, and find a design guideline for developing the THz materials. In this report, we investigate the antiferromagnetic resonance properties in the cation substituted NiO of $Ni_{1-x}M_xO$ (M = Mn, Li, or Mg). It is shown that the cation substitution enables a wide range control of the antiferromagnetic resonant frequency as well as of the Q factor. We also discuss distinct effects of the magnetic doping (Mn^{2+}), nonmagnetic doping (Mg^{2+}), and hole doping (Li^{1+}) on the antiferromagnetic resonance properties.

The antiferromagnetic resonance frequency ω_r is described as [30,31]

$$\omega_r = \gamma\sqrt{2H_E H_A}, \tag{1}$$

where $\gamma = 1.76 \times 10^{11}\,\mathrm{T^{-1}\,s^{-1}}$ is the gyromagnetic ratio, H_E is the molecular field due to the exchange interaction between the magnetic sites, and H_A is the magnetic anisotropy field. Here, we assume that $H_E \gg H_A$ with the typical values for antiferromagnet $H_E \sim 1000$ T and $H_A \sim 1$ T. Because the large H_E comes into play in the resonant frequency, the

*Corresponding author: mtaka@scl.kyoto-u.ac.jp

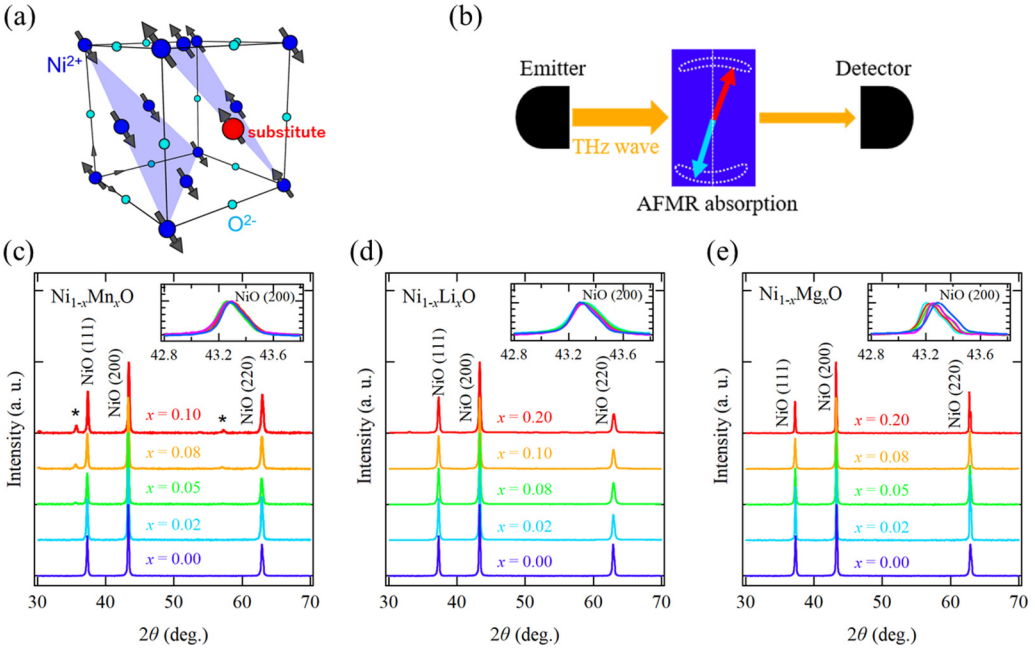

FIG. 1. (a) Crystalline and magnetic structure of NiO with a cation substitution indicated with the red ion. (b) Schematic illustration of the THz transmission measurement on an antiferromagnet sample. Persistent magnetization dynamics is excited at the antiferromagnetic resonant frequency and therefore the THz waves are absorbed. The x-ray diffraction for (c) $Ni_{1-x}Mn_xO$, (d) $Ni_{1-x}Li_xO$, and (e) $Ni_{1-x}Mg_xO$. Peaks due to the pure NiO are indexed. Other peaks labeled by * are due to impurity phases of $MnNi_2O_4$.

antiferromagnetic resonance occurs at much higher frequency, i.e., ∼THz, than the ferromagnetic resonance (∼GHz), which is determined only by H_A [32]. For a pure NiO, the resonant frequency is typically observed around 1 THz [14,18,33,34]. In a general definition, the Q factor $Q$is obtained by

$$Q = \omega_r/\Delta\omega, \tag{2}$$

where the linewidth $\Delta\omega$ is the full width at half maximum of the resonant absorption peak.

Sintered pellet samples of $Ni_{1-x}M_xO$, employed in the experiments, were made from mixtures of NiO, MnO, Li_2O, and MgO powders (purity 99.97% and the average grain size of 7 μm). The composition of each sample was controlled by adjusting the amount of the powders to the target ratio. The powders were mixed in a mortar for 30 min and prefired at 1473 K for 3 h. The sample was milled again in a mortar for 30 min and uniaxially diepressed with a force of 750 kgf applied onto 100 mm^2 to form a ∼5-mm-diameter and ∼3-mm-thick pellet. The pellet was then sintered at 1773 K for 2 h in air to solidify. THz wave transmission through the samples was measured by using a frequency domain continuous wave (CW)-THz spectroscopy system [18] capable of scanning up to $\omega = 2$ THz with the frequency resolution <10 MHz as the schematic illustration is shown in Fig. 1(b). The absorption peak due to the antiferromagnetic resonance is expected in the transmission spectra. Sample temperature during the measurement can be controlled between 77 and 450 K. We apply no magnetic field in the measurements. Magnetic susceptibility measurements were performed as a function of temperature in order to determine the Néel temperature T_N. X-ray diffraction was performed with the Cu Kα radiation to characterize the crystalline structure at room temperature.

The x-ray diffraction shown in Figs. 1(c)–1(e) indicates that a single phase of the NiO structure (point group: $\bar{3}m$) is maintained with up to $x = 0.20$ except for the case of $Ni_{1-x}Mn_xO$ samples. For the Mn^{2+} substitution, the second phase identified with $MnNi_2O_4$ spinel, labeled as * in Fig. 1(c), appears with $x > 0.05$. While no appreciable variations in the lattice parameter of the NiO crystalline phase were seen in the $Ni_{1-x}Mn_xO$ and the $Ni_{1-x}Li_xO$ samples, the lattice contraction of 0.2% with $x = 0.20$ is observed for the $Ni_{1-x}Mg_xO$ samples [see the inset of Figs. 1(c)–1(e)], which is in agreement with the previous reports [26,27].

Figure 2 shows the transmission spectra of the THz waves as function of frequency and temperature. A sharp absorption at about 1.1 THz at 77 K is clearly seen in the sample with $x = 0.00$, indicating the antiferromagnetic resonance are excited at that frequency at that temperature. The resonant frequency gradually decreases with increasing the temperature with fairly good frequency tunability 1∼0.8 THz in the temperature range of 77∼450 K. The effect of the cation substitution is quite obvious in the resonant frequency. There is a tendency of decreasing the resonant frequency with increasing x for all the samples and the absorption peaks eventually fade out with large x. It is worth noting that the THz transmission for the $Ni_{1-x}Li_xO$ samples rapidly drops at a high frequency because the Li^+ substitution increases the electrical conductivity and therefore increases the reflectivity for the electromagnetic wave due to the skin effect. As the conductivity further increases with temperature, the significant reflectivity hinders the absorption peaks at higher temperature. Nevertheless, the absorption at 300 K is still clearly visible (see also Fig. 5 for frequency scanned spectra).

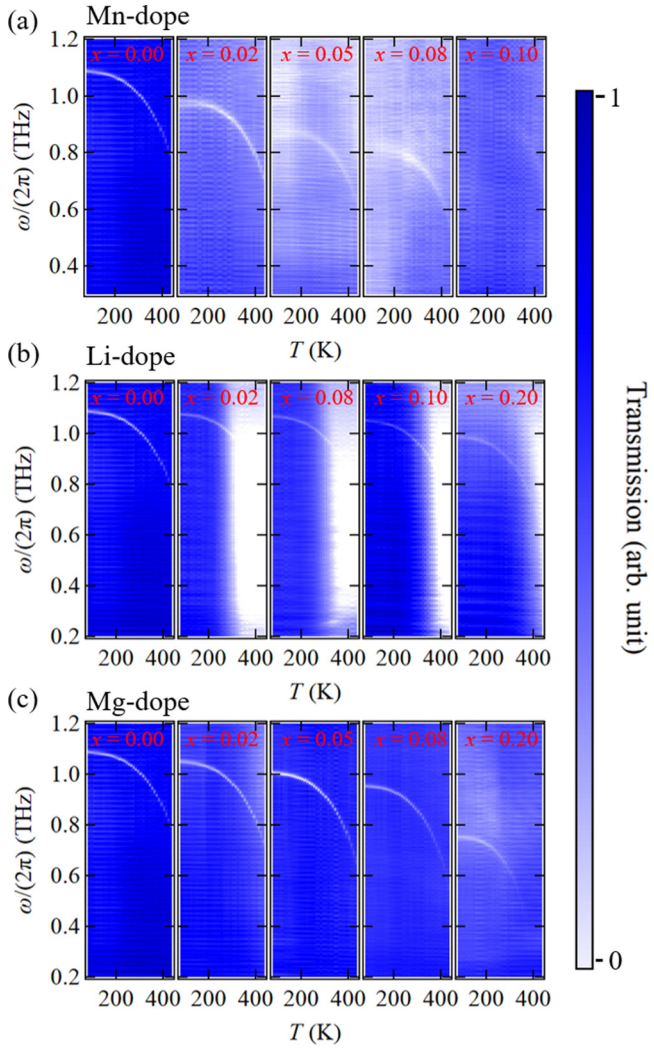

FIG. 2. Transmission of the THz wave as functions of frequency and temperature for (a) $Ni_{1-x}Mn_xO$, (b) $Ni_{1-x}Li_xO$, and (c) $Ni_{1-x}Mg_xO$ with various x.

From the temperature dependence of the resonant frequency shown in Fig. 3, the resonant frequency at 0 K, ω_0, representing the intrinsic resonance of the system can be estimated by the equation [14,15,18] $\omega_r = \omega_0(M_0'(T))^n$ with a given T_N, where $M_0'(T)$ is the normalized sublattice magnetization computed by the Brillouin function $B_{S=1}(T)$ and n is the empirical exponent [18]. Here, we fit the data with the equation by setting ω_0 and n the fitting parameters with T_N obtained from the susceptibility measurements (see the Supplemental Material [35]). We note that $n = 0.72$ [18] fits very well for $Ni_{1-x}Li_xO$ and $Ni_{1-x}Mg_xO$ while $n = 0.61$ was obtained for $Ni_{1-x}Mn_xO$. Figure 4 summarizes ω_0 and T_N as a function of x. As one already perceived in Fig. 3, both ω_0 and T_N monotonically decrease with x except for the $Ni_{1-x}Mn_xO$ sample with the highest substitution of $x = 0.10$, which could be associated with the emergence of the $MnNi_2O_4$ phase. In the following paragraphs, behaviors of ω_0 and T_N and their correlation will be discussed in more detail for each cation substitution. According to Eq. (1) (with $\omega_0 = \omega_r$), the antiferromagnetic resonant frequency is determined by the two magnetic parameters, H_A and H_E. Given that the crystalline symmetry and the coordination numbers are barely changed with the doping, we can presume that H_E is proportional to T_N in the framework of the molecular field theory [20]. Therefore, the obtained T_N variation can be directly mapped to the variation of H_E.

In the case of the $Ni_{1-x}Mn_xO$ samples with $0.00 \leqslant x \leqslant 0.08$, ω_0 decreases with x more rapidly than T_N. ω_0 decreases at the rate of 24% while T_N decreases at the rate of 6% in $0.00 \leqslant x \leqslant 0.08$. Considering the square root on $H_E(\equiv T_N)$ in Eq. (1), the decrease of ω_0 is influenced more by a reduction of the anisotropy field H_A with increasing x rather than the reduction of T_N. The main effect of the Mn^{2+} substitution on the antiferromagnetic resonance is thus the reduction of the magnetic anisotropy of the NiO. The frequency tunability with respect to x is found to be the largest among all the sample $\omega_0/x = 2\pi \times 3.2$ THz in $0.00 \leqslant x \leqslant 0.08$. In the case of the $Ni_{1-x}Li_xO$ samples, both ω_0 and T_N only slightly decrease at the similar rate with 9% for ω_0 and 7% for T_N in $0.00 \leqslant x \leqslant 0.20$. Based on Eq. (1), this basically suggests that both the weakening of H_E and the reduction of the anisotropy field H_A almost equally contribute to the ω_0 reduction. The frequency tunability is found to be the smallest $\omega_0/x = 2\pi \times 0.4$ THz in $0.00 \leqslant x \leqslant 0.20$. In the case of the $Ni_{1-x}Mg_xO$ samples, ω_0 and T_N decrease more rapidly than the ones for the $Ni_{1-x}Li_xO$ samples. The decrease rate was 30% for ω_0 and 22% for T_N in $0.00 \leqslant x \leqslant 0.20$, suggesting in the same way as the $Ni_{1-x}Li_xO$ case that both H_E and H_A reductions contribute to

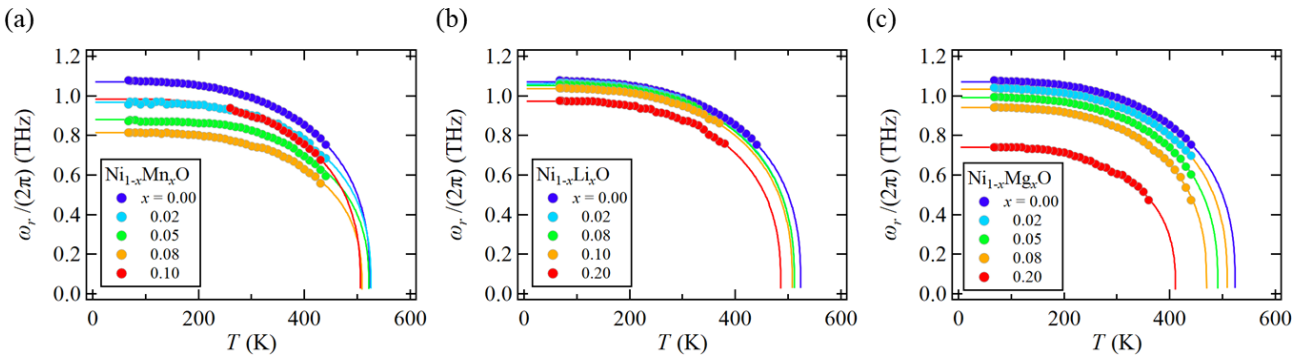

FIG. 3. Temperature dependence of the resonant frequency for (a) $Ni_{1-x}Mn_xO$, (b) $Ni_{1-x}Li_xO$, and (c) $Ni_{1-x}Mg_xO$ with various x.

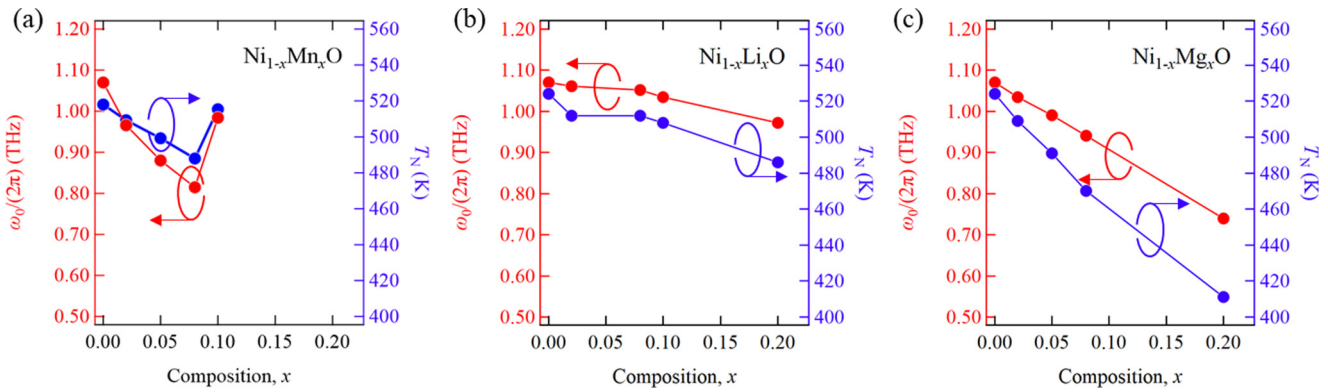

FIG. 4. $\omega_0/(2\pi)$ and T_N as a function of composition x for (a) $Ni_{1-x}Mn_xO$, (b) $Ni_{1-x}Li_xO$, and (c) $Ni_{1-x}Mg_xO$.

the ω_0 reduction. The large decrease rate of T_N, or H_E, can be explained by the drastic weakening of the superexchange interaction by Mg^{2+} substitution due to suppression of the electron orbital correlation between the atomic sites [27] which can originate from the lattice contraction [29] [see Fig. 1 (e)]. The frequency tunability is found to be $\omega_0/x = 2\pi \times 1.6\,\mathrm{THz}$ in $0.00 \leqslant x \leqslant 0.20$.

Lastly, we discuss the Q factor of those samples. Figure 5 displays the transmission spectra as a function of frequency at 300 K. While a little increase in the linewidth $\Delta\omega$ with increasing x [see Fig. 5(d)] for the $Ni_{1-x}Li_xO$ and $Ni_{1-x}Mg_xO$ samples, the significantly large broadening of $\Delta\omega$ with respect to x is observed for the $Ni_{1-x}Mn_xO$ samples. In accordance with the x dependence of $\Delta\omega$, the Q factor evaluated by Eq. (2) is the smallest with the Mn^{2+} substitution among all the samples and decreases rather drastically with increasing x. In general, the linewidth, or the Q factor, of the magnetic resonance can vary due to various spin relaxation mechanisms that may be intrinsic to the materials or may be extrinsic by magnetic inhomogeneity of the material, distribution of the magnetic anisotropy, etc. [18]. One possible mechanism of the Q factor degradation in the $Ni_{1-x}Mn_xO$ samples could be due to the introduction of the magnetic inhomogeneity by a different species of the magnetic ion, i.e., Mn^{2+}. The influence of the parasitic $MnNi_2O_4$ spinel phase should also be considered for the linewidth broadening. More in-depth physical understanding of the antiferromagnetic damping, leading to the resonant linewidth and the Q factor, requires a development of microscopic spin relaxation theories similar to those for ferromagnets [36,37].

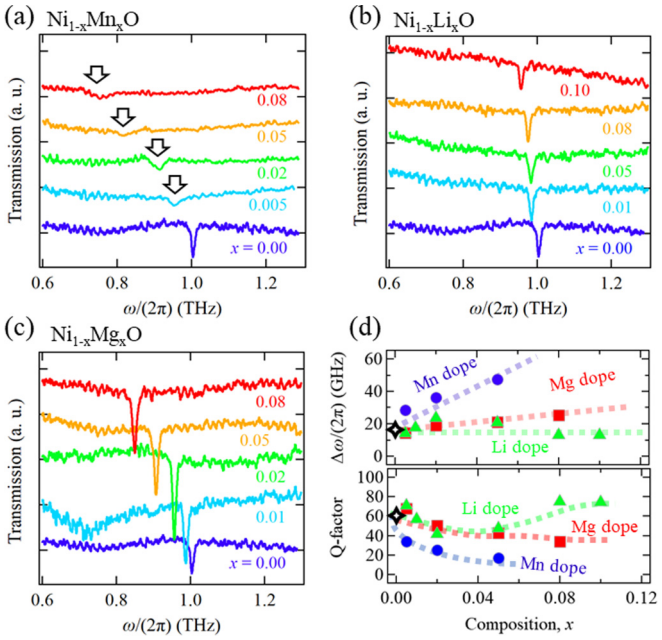

FIG. 5. The transmission spectra at 300 K for (a) $Ni_{1-x}Mn_xO$, (b) $Ni_{1-x}Li_xO$, and (c) $Ni_{1-x}Mg_xO$. The arrows indicate the position of the absorption peaks (d) $\Delta\omega/(2\pi)$ and the Q factor as a function of composition x. (✧) denotes the pure NiO. The dotted curves are a guide for the eye.

In summary, we investigated the antiferromagnetic resonance in the cation-substituted NiO of $Ni_{1-x}M_xO$ (M = Mn, Li, or Mg). We show the wide range tunability of the resonant frequency as well as the Q factor by the magnetic doping (Mn^{2+} substitute), the nonmagnetic doping (Mg^{2+} substitute), and the hole doping (Li^+ substitute). We discussed the trends of how those different dopings impact the antiferromagnetic resonance properties, which will be appreciated as a design guideline for THz materials adapting to various types of applications such as THz microwave absorbers and filters where the control of ω_r and Q factor is important. Moreover, our work presented here should stimulate more extensive exploration of antiferromagnets as THz materials from both experimental and theoretical sides. In particular, we expect extended *ab initio* studies [38] to address and predict properties of both the electric and the THz magnetic dynamics and their correlations in those doped antiferromagnetic oxide systems. Our work with those perspectives opens up a different avenue of study on antiferromagnetic THz materials.

We thank K. Nakamura at Mie University for a fruitful discussion. This work was supported in part by JSPS KAKENHI Grants No. 17H04924, No. 15H05702, No. 17H04795, No. 17H05181 ("Nano Spin Conversion Science"), and by the Collaborative Research Program of Institute for Chemical Research, Kyoto University (Grant No. 2018–61).

[1] J. Walowski and M. Münzenberg, Perspective: Ultrafast magnetism and THz spintronics, J. Appl. Phys. **120**, 140901 (2016).

[2] D. M. Mittleman, Perspective: Terahertz science and technology, J. Appl. Phys. **122**, 230901 (2017).

[3] A. N. Yusoff, M. H. Abdullah, S. H. Ahmad, S. F. Jusoh, A. A. Mansor, and S. A. A. Hamid, Electromagnetic and absorption properties of some microwave absorbers, J. Appl. Phys. **92**, 876 (2002).

[4] K. David and H. Berndt, 6G vision and requirements, IEEE Veh. Technol. Mag. **13**, 72 (2018).

[5] T. Jungwirth, X. Marti, P. Wadley, and J. Wunderlich, Antiferromagnetic spintronics, Nat. Nanotechnol. **11**, 231 (2016).

[6] V. Baltz, A. Manchon, M. Tsoi, T. Moriyama, T. Ono, and Y. Tserkovnyak, Antiferromagnetic spintronics, Rev. Mod. Phys. **90**, 015005 (2018).

[7] T. Kampfrath, T. Jungwirth, V. Novák, P. Wadley, R. P. Campion, P. Kužel, T. Seifert, P. Němec, M. Baumgartner, Z. Kašpar, J. Sinova, P. Gambardella, J. Wunderlich, M. Müller, and K. Olejník, Terahertz electrical writing speed in an antiferromagnetic memory, Sci. Adv. **4**, eaar3566 (2018).

[8] R. Cheng, D. Xiao, and A. Brataas, Terahertz Antiferromagnetic Spin Hall Nano-Oscillator, Phys. Rev. Lett. **116**, 207603 (2016).

[9] R. Khymyn, I. Lisenkov, V. Tiberkevich, B. A. Ivanov, and A. Slavin, Antiferromagnetic THz-frequency Josephson-like oscillator driven by spin current, Sci. Rep. **7**, 43705 (2017).

[10] M. van Veenendaal, Competition between screening channels in core-level x-ray photoemission as a probe of changes in the ground-state properties of transition-metal compounds, Phys. Rev. B **74**, 085118 (2006).

[11] M. Taguchi, M. Matsunami, Y. Ishida, R. Eguchi, A. Chainani, Y. Takata, M. Yabashi, K. Tamasaku, Y. Nishino, T. Ishikawa, Y. Senba, H. Ohashi, and S. Shin, Revisiting the Valence-Band and Core-Level Photoemission Spectra of NiO, Phys. Rev. Lett. **100**, 206401 (2008).

[12] N. F. Mott, The basis of the electron theory of metals, with special reference to the transition metals, Proc. Phys. Soc. London, Sect. A **62**, 416 (1949).

[13] J. Hubbard, Electron correlations in narrow energy bands, Proc. R. Soc. London, Ser. A **276**, 238 (1963).

[14] M. Tinkham, Far infrared spectra of magnetic materials, J. Appl. Phys. **33**, 1248 (1962).

[15] A. Sievers and M. Tinkham, Far infrared antiferromagnetic resonance in MnO and NiO, Phys. Rev. **129**, 1566 (1963).

[16] M. T. Hutchings and E. J. Samuelsen, Measurement of spin-wave dispersion in NiO by inelastic neutron scattering and its relation to magnetic properties, Phys. Rev. B **6**, 3447 (1972).

[17] J. Zaanen, G. A. Sawatzky, and J.W. Allen, Band Gaps and Electronic Structure of Transition-Metal Compounds, Phys. Rev. Lett. **55**, 418 (1985).

[18] T. Moriyama, K. Hayashi, K. Yamada, M. Shima, Y. Ohya, and T. Ono, Intrinsic and extrinsic antiferromagnetic damping in NiO, Phys. Rev. Mater. **3**, 051402 (2019).

[19] T. Moriyama, K. Hayashi, K. Yamada, M. Shima, Y. Ohya, Y. Tserkovnyak, and T. Ono, Enhanced antiferromagnetic resonance linewidth in NiO/Pt and NiO/Pd, Phys. Rev. B **101**, 060402 (2020).

[20] P. W. Anderson, Generalizations of the Weiss molecular field theory of antiferromagnetism, Phys. Rev. **79**, 705 (1950).

[21] S. Hüfner, Electronic structure of NiO and related 3*d*-transition-metal compounds, Adv. Phys. **43**, 183 (1994).

[22] Michael D. Irwin, D. Bruce Buchholz, Alexander W. Hains, Robert P. H. Chang, and Tobin J. Marks, p-Type semiconducting nickel oxide as an efficiency-enhancing anode interfacial layer in polymer bulk-heterojunction solar cells, PNAS **105**, 2783 (2008).

[23] H. Ohta, M. Hirano, K. Nakahara, H. Maruta, T. Tanabe, M. Kamiya, T. Kamiya, and H. Hosono, Fabrication and photoresponse of a pn-heterojunction diode composed of transparent oxide semiconductors, p-NiO and, Appl. Phys. Lett. **83**, 1029 (2003).

[24] J. B. Goodenough, D. G. Wickham, and W. J. Croft, Some magnetic and crystallographic properties of the system $Li^{+}_{x}Ni^{++}_{1-2x}ni^{+++}_{x}O$, J. Phys. Chem. Solids **5**, 107 (1958).

[25] J. Y. Zhang, W. W. Li, R. L. Z. Hoye, J. L. MacManus-Driscoll, M. Budde, O. Bierwagen, L. Wang, Y. Du, M. J. Wahila, L. F. J. Piper, T.-L. Lee, H. J. Edwards, V. R. Dhanakg, and K. H. L. Zhang, Electronic and transport properties of Li-doped NiO epitaxial thin films, J. Mater. Chem. C **6**, 2275 (2018).

[26] R. C. Boutwell, M. Wei, A. Scheurer, J. W. Mares, and W. V. Schoenfeld, Optical and structural properties of NiMgO thin films formed by sol–gel spin coating, Thin Solid Films **520**, 4302 (2012).

[27] Y. Chen, O. Sakata, R. Yamauchi, A. Yang, L. S. R. Kumara, C. Song, N. Palina, M. Taguchi, T. Ina, Y. Katsuya, H. Daimon, A. Matsuda, and M. Yoshimoto, Lattice distortion and electronic structure of magnesium-doped nickel oxide epitaxial thin films, Phys. Rev. B **95**, 245301 (2017).

[28] A. E. Hughes, Antiferromagnetic resonance in MnO: Co: A measurement of the magnetoelastic properties of the Co^{2+} ion, Phys. Rev. B **3**, 877 (1971).

[29] E. Cazzanelli, A. Kuzmin, N. Mironova-Ulmane, and G. Mariotto, Behavior of one-magnon frequency in antiferromagnetic $Ni_cMg_{1-c}O$ solid solutions, Phys. Rev. B **71**, 134415 (2005).

[30] C. Kittel, Theory of antiferromagnetic resonance, Phys. Rev. **82**, 565 (1951).

[31] T. Nagamiya, Theory of antiferromagnetism and antiferromagnetic resonance absorption, Prog. Theoret. Phys. (Kyoto) **6**, 342 (1951).

[32] C. Kittel, On the theory of ferromagnetic resonance absorption, Phys. Rev. **73**, 155 (1948).

[33] T. Kampfrath, A. Sell, G. Klatt, A. Pashkin, S. Meahrlein, T. Dekorsy, M. Wolf, M. Fiebig, A. Leitenstorfer, and R. Huber, Coherent terahertz control of antiferromagnetic spin waves, Nat. Photon. **5**, 31 (2011).

[34] T. Satoh, S.-J. Cho, R. Iida, T. Shimura, K. Kuroda, H. Ueda, Y. Ueda, B. A. Ivanov, F. Nori, and M. Fiebig, Spin Oscillations in Antiferromagnetic NiO Triggered by Circularly Polarized Light, Phys. Rev. Lett. **105**, 077402 (2010).

[35] See Supplemental Material at http://link.aps.org/supplemental/10.1103/PhysRevMaterials.4.074402 for details on determination of the Néel temperature.

[36] V. Kamberský and C. E. Patton, Spin-wave relaxation and phenomenological damping in ferromagnetic resonance, Phys. Rev. B **11**, 2668 (1975).

[37] N. Smith, Fluctuation–dissipation considerations for phenomenological damping models for ferromagnetic thin films, J. Appl. Phys. **92**, 3877 (2002).

[38] M. D. Towler, N. L. Allan, N. M. Harrison, V. R. Saunders, W.C. Mackrodt, and E. Apra, *Ab initio* study of MnO and NiO, Phys. Rev. B **50**, 5041 (1994).